LETTER • OPEN ACCESS

Nowcasting tracks of severe convective storms in West Africa from observations of land surface state

To cite this article: Christopher M Taylor *et al* 2022 *Environ. Res. Lett.* **17** 034016

View the article online for updates and enhancements.

ENVIRONMENTAL RESEARCH
LETTERS

CrossMark

LETTER

Nowcasting tracks of severe convective storms in West Africa from observations of land surface state

Christopher M Taylor[1,2] ⓘ, Cornelia Klein[1,3] ⓘ, Cheikh Dione[4] ⓘ, Douglas J Parker[5,6] ⓘ, John Marsham[5] ⓘ, Cheikh Abdoulahat Diop[7] ⓘ, Jennifer Fletcher[5] ⓘ, Abdoul Aziz Saidou Chaibou[8] ⓘ, Dignon Bertin Nafissa[8], Valiyaveetil Shamsudheen Semeena[1] ⓘ, Steven J Cole[1] ⓘ and Seonaid R Anderson[1] ⓘ

[1] UK Centre for Ecology and Hydrology, Wallingford, United Kingdom
[2] National Centre for Earth Observation, Wallingford, United Kingdom
[3] Department of Atmospheric and Cryospheric Sciences, University of Innsbruck, Innsbruck, Austria
[4] African Centre of Meteorological Applications for Development (ACMAD), Niamey, Niger
[5] Institute for Climate and Atmospheric Science, University of Leeds, Leeds, United Kingdom
[6] NORCE Norwegian Research Center, Bjerknes Center for Climate Research, Bergen, Norway
[7] Agence Nationale de l'Aviation Civile et de la Météorologie, Dakar, Senegal
[8] Direction de la Météorologie Nationale, Niamey, Niger

E-mail: cmt@ceh.ac.uk

Abstract

In tropical convective climates, where numerical weather prediction of rainfall has high uncertainty, nowcasting provides essential alerts of extreme events several hours ahead. In principle, short-term prediction of intense convective storms could benefit from knowledge of the slowly evolving land surface state in regions where soil moisture controls surface fluxes. Here we explore how near-real time (NRT) satellite observations of the land surface and convective clouds can be combined to aid early warning of severe weather in the Sahel on time scales of up to 12 h. Using land surface temperature (LST) as a proxy for soil moisture deficit, we characterise the state of the surface energy balance in NRT. We identify the most convectively active parts of mesoscale convective systems (MCSs) from spatial filtering of cloud-top temperature imagery. We find that predictive skill provided by LST data is maximised early in the rainy season, when soils are drier and vegetation less developed. Land-based skill in predicting intense convection extends well beyond the afternoon, with strong positive correlations between daytime LST and MCS activity persisting as far as the following morning in more arid conditions. For a Forecasting Testbed event during September 2021, we developed a simple technique to translate LST data into NRT maps quantifying the likelihood of convection based solely on land state. We used these maps in combination with convective features to nowcast the tracks of existing MCSs, and predict likely new initiation locations. This is the first time to our knowledge that nowcasting tools based principally on land observations have been developed. The strong sensitivity of Sahelian MCSs to soil moisture, in combination with MCS life times of typically 6–18 h, opens up the opportunity for nowcasting of hazardous weather well beyond what is possible from atmospheric observations alone, and could be applied elsewhere in the semi-arid tropics.

1. Introduction

Soil moisture provides a potential source of predictability for rainfall in many regions and seasons [1–4]. These 'hotspots' of soil moisture-precipitation feedback require two conditions to be met. Firstly, soil moisture deficits must exert a strong control on the partition of surface energy into sensible and latent heat fluxes [5, 6]. Secondly, the atmosphere must be able to support deep convection given favourable land surface fluxes [7]. An ensemble of global forecast models showed that during boreal summer, these conditions are met in regions such as India and the US Great Plains [3], when soil

moisture deficits coincide with periods of convective rainfall.

The African Sahel also satisfies these criteria, and according to global observational analyses [4, 8], provides the clearest evidence of soil moisture-precipitation feedbacks in operation. The concentration of annual rain within the months of June–September gives rise to sparse, rapidly developing vegetation cover, where surface energy balance dynamics are dominated by the presence of near surface soil moisture from rain in the previous two to three days [9]. The vast majority of Sahel rainfall is produced by mesoscale convective systems (MCSs) [10, 11]. These systems typically initiate during the afternoon and travel westwards overnight given strong wind shear and convective instability. Longer-lived MCSs leave swaths of wet soil hundreds of kilometres long, resetting surface flux patterns the following day.
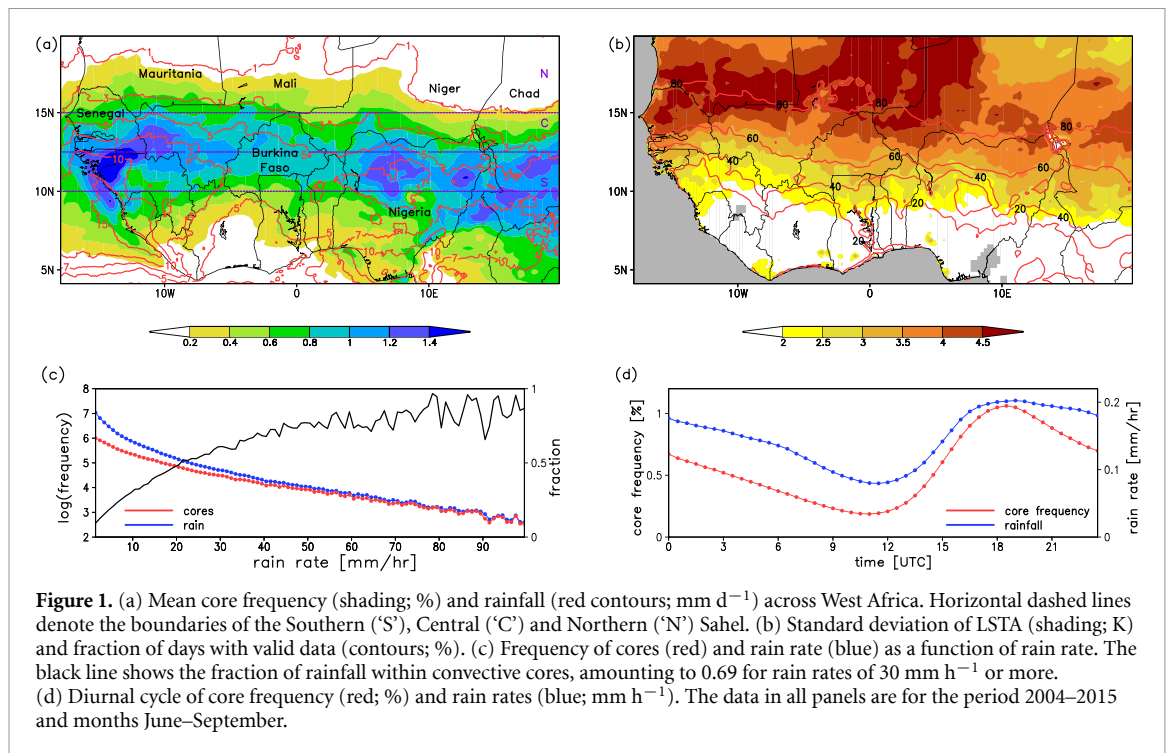
The largely flat terrain and (unlike in India and the Great Plains) the absence of extensive irrigation thus make the Sahel a perfect 'natural laboratory' to observe soil moisture-precipitation feedbacks. On scales of the order of 10 km upwards, soil moisture patterns drive daytime circulations [12] which favour the initiation of MCSs [13, 14]. Over several hundred kilometres, propagating MCSs tend to intensify over drier surfaces [15; hereafter KT20], particularly in late afternoon and early evening, whilst wetter surfaces suppress convection, an effect which is evident throughout the night. KT20 illustrated the important influence of large-scale soil moisture gradients on the dynamics of the atmosphere, modifying MCS-enhancing regional moisture convergence and wind shear. Zonal soil moisture structures created by long-lived MCSs in previous days affect both the location of the inter-tropical discontinuity (ITD), where moist south-westerly monsoon winds meet dry air coming down from the Sahara, and the strength of the African easterly jet (AEJ) [16]. MCS activity is enhanced in the presence of the ITD due to moisture convergence [17], whilst enhanced wind shear associated with the AEJ helps to organise MCSs [18]. Moreover at synoptic scales, soil moisture-modulated heating directly feeds back on wave structures in which convection is embedded [19, 20].

These research studies raise the question of whether knowledge of the land surface state can improve MCS predictions in near-real time (NRT). There is an urgent need for reliable forecasts of severe storms here as their intense rain and high winds can be extremely damaging. The rapid expansion of urban areas across the region, often with inadequate drainage networks, is driving increased damages from flash flooding [21]. In the context of climate change, this issue is worsening as the region has already seen a rapid increase in the frequency of the most intense MCSs [18, 22], and this trend is expected to continue [23, 24]. Rainfall predictions

from current global ensemble numerical modelling systems have low skill, failing to outperform climatology in West and Central Africa, even after postprocessing of model outputs [25]. The low skill of model forecasts is due to a combination of weak synoptic forcing, limited observations for data assimilation, and the rapid development of MCSs, which dominate the growth of model errors [26]. Indeed a recent study highlighted how a statistical model based simply on past rainfall observations consistently outperforms a state-of-the-art global ensemble prediction system [27].

The rapid growth and longevity of MCSs means that NRT rainfall forecasts need to incorporate the current locations of active convection and preconvective instabilities. This remains challenging for Numerical Weather Prediction (NWP) systems [28, 29], even in regions with substantially more observations and computer resources for rapid data assimilation [30, 31]. In the absence of reliable NWP, extrapolation-based nowcasting is a vital forecasting method. This involves making predictions on time scales of hours based on observations of existing weather systems from weather radar and/or thermal-infrared imagery by tracking and extrapolating storm trajectories [32–34], including deep learning approaches [35, 36] and in combination with NWP [37]. In many parts of the world (e.g. Tornado Alley in the US) such approaches provide a lifesaving service. Nowcasting thus forms an important element of the African Science for Weather Information and Forecasting Techniques (SWIFT) [38]. In West Africa, there are currently no operational ground-based weather radars. Imagery from geostationary satellites is therefore crucial in identifying active MCSs. Operational forward-tracking of satellite imagery has skill out to at least 90 min in the region [39], whilst new techniques indicate an extension of skill out to at least 4 h [40]. Predictability from extrapolation of existing systems is stronger overnight, when larger, organised and long-lived systems dominate. During the daytime, the combination of smaller, short-lived systems and frequent new initiations make forward-tracking less effective. However, daytime is also when land surface effects on MCSs are expected to be maximised. This raises the possibility of using information on land surface state to improve short-term predictions of hazardous weather.

In this paper, we explore how to bring together NRT satellite observations of the land surface and clouds to increase skill in predicting hazardous long-lived storms in the Sahel. We focus on nowcasting time scales, conventionally taken to be 0–6 h [41]. With additional land surface-derived skill however, we extend this scale to 12 h. To our knowledge, this is the first attempt anywhere to build nowcasting tools based primarily on the use of land surface information. In the next section, we describe the observational datasets and methods. Section 3

Figure 1. (a) Mean core frequency (shading; %) and rainfall (red contours; mm d^{-1}) across West Africa. Horizontal dashed lines denote the boundaries of the Southern ('S'), Central ('C') and Northern ('N') Sahel. (b) Standard deviation of LSTA (shading; K) and fraction of days with valid data (contours; %). (c) Frequency of cores (red) and rain rate (blue) as a function of rain rate. The black line shows the fraction of rainfall within convective cores, amounting to 0.69 for rain rates of 30 mm h^{-1} or more. (d) Diurnal cycle of core frequency (red; %) and rain rates (blue; mm h^{-1}). The data in all panels are for the period 2004–2015 and months June–September.

presents the key results, quantifying the sensitivity of convection to surface variability at different times of day and different months. We then describe the application of a prototype system during a recent SWIFT 'Forecasting Testbed' (13–24 September 2021), an event where operational forecasters and researchers came together to test out new forecasting methods, in collaboration with user groups.

2. Data

We focus on the West African Monsoon, spanning the months June–September (JJAS), and in particular consider the latitudes 10–20° N, comprising the Southern, Mid- and Northern Sahel (figure 1(a)). A strong meridional rainfall gradient characterises the Sahel, with JJAS-mean rain ranging from ∼7 mm d^{-1} in the Southern Sahel to less than 1 mm d^{-1} at 20° N. We develop statistical relationships between the land and convection over a 12 year historical period and test them out during the SWIFT Testbed.

We use data from the Spinning Enhanced Visible and Infrared Imager (SEVIRI) on board the Meteosat Second Generation series of satellites. This provides images every 15 min from 12 channels at a spatial resolution of around 3 km over our domain with a latency of 30 min. For analysing deep convection, following [42] we filter the cloud-top temperature field from the 10.8 μm channel to identify the coldest features on scales of 9–130 km, which we term 'convective cores'. This approach removes often-extensive cold cloud shields, where rain rates tend to be light, as well as features on sub-9 km scales, which likely have limited predictability within an MCS. Figure 1(c)

illustrates the frequency distribution of convective cores as a function of rain rate, as provided by IMERG high quality precipitation estimates from microwave sensors on board polar-orbiting satellites. This confirms that the presence of a core indicates a high likelihood of intense convective rainfall.

To characterise the land surface state, we use land surface temperature (LST) observations derived from the 10.8 and 12 μm SEVIRI channels [43] under clear skies. In semi-arid regions, many studies have shown that daytime LST provides a proxy for soil moisture stress [44–47]; when soils are drier, evapotranspiration (ET) is constrained, and LST rises along with sensible heat flux and longwave emission. We use LST, rather than microwave-based soil moisture, due to the high sampling frequency, low latency, and relatively high spatial resolution of the SEVIRI LST product. We note that in the Sahel, the land and atmosphere are tightly coupled on multiple scales [12, 15, 19] and therefore maps of LST implicitly contain information on atmospheric as well as land surface states. We use LST data provided by the Satellite Application Facility on Land Surface Analysis (https://landsaf.ipma.pt). This includes both their archived data record (2004–2015), which defines our 12 year historical period, and their NRT product. We apply additional screening based on the temporal evolution of LST at each pixel [13]. This involves removing pixels with sub-hourly LST fluctuations, which are typically produced by undiagnosed clouds. For each cloud-free pixel and 15 min image, LST anomalies (LSTAs) are computed relative to a 12 year climatology within a moving window of 31 days. We then take the pre-convection daytime average LSTA of all images starting from 0700 UTC on the day of

interest. The use of LSTAs allows us to focus on transient variations in the surface energy balance, which are dominated by soil moisture fluctuations in a semiarid region. We also apply a spatial wavelet decomposition to the LSTA field to quantify length scales of variability from 20 to 320 km. To facilitate comparison across length scales, we normalise wavelet coefficients by their standard deviations. To illustrate the relationship between LSTA and surface wetness, we compare with soil moisture at the 0.25° scale derived from Numerical Weather Prediction (AMSR-E) [48] for the years 2004–2011.

The standard deviation of daily LSTA (figure 1(b)) illustrates key aspects of land surface behaviour across the Sahel. Day-to-day variability in LSTA is smallest in the south, where soil moisture control on ET is weak [9], and the well-vegetated surface is aerodynamically rougher. Fluctuations in LSTA increase rapidly moving north, peaking in the Northern Sahel. The maximum occurs where intermittent rainfall coincides with very sparse vegetation cover, roughly bounded in the north by the 1 mm d^{-1} isohyet (figure 1(a)). Note that cloud cover limits the availability of LST data, with relatively more cloudy days in the south (figure 1(b)), particularly at the height of the monsoon season.
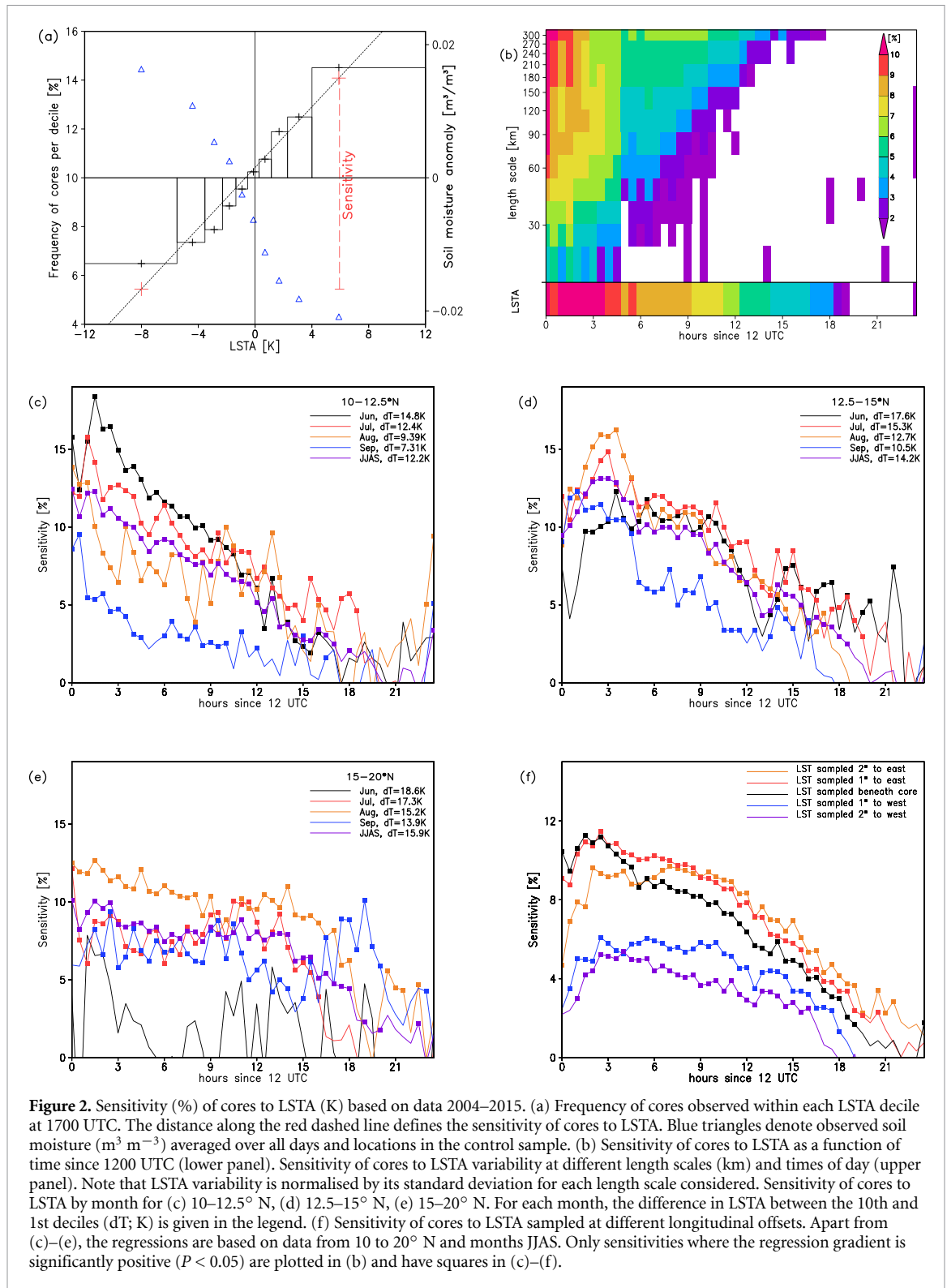
3. Statistical relationships

We first develop climatological relationships between antecedent LSTA and the likelihood of a convective core, for application in NRT. For each 30 min period of the day within the historical period, we create a 'cores' sample of LSTAs, which lie beneath the maximum wavelet power in each convective core. For cores observed between 1200 and 1700 UTC we use LSTA data created from an average of all images between 0700 and 1200 UTC on that day, and for subsequent hours (including the following morning) we use the LSTA based on images from 0700 to 1700 UTC. We compare this with a 'control' dataset consisting of LSTAs sampled at the same location and day of year but in the remaining 11 years. We use the latter to determine the expected statistical distribution of LSTAs given the space-time sampling of convection. For example, during June there will be a larger contribution to the control sample from the Southern Sahel, where storms are more frequent at that time of year. For each decile in the control distribution, we compute the frequency of observed cores, and regress these ten values against the mean LSTA within each decile. Figure 2(a) illustrates this relationship for all 19 908 Sahelian convective cores observed at 1700 UTC. If there were no relationship between LSTA and convection, the frequency of cores observed within each decile would be approximately 10%. Instead, there is a strong positive correlation. We define the sensitivity to LSTA as the difference

in core frequency between the tenth and first LSTA deciles, which in this case equals 8.6%. Qualitatively this strong sensitivity is consistent with previous studies which have shown that convection is favoured over drier (and warmer) surfaces, whether that convection be newly initiated [13] or within propagating MCSs (KT20). Because the land and atmosphere are tightly coupled, the sensitivity metric implicitly incorporates information on the atmosphere, for example through the creation of synoptic scale soil moisture structures by African easterly waves [19, 20].

We would expect sensitivity of convective cores to LSTA to be strong during the afternoon, when the planetary boundary layer is well-developed, and its spatial variability is dominated by daytime flux patterns. However, figure 2(b) illustrates that a significantly positive relationship ($P < 0.05$) is found from midday through to 0800 UTC the following day. In other words, even 12 h after sunset (average time of 1800 UTC), there is still inherent predictability of convection from the previous day's LSTA. Figure 2(b) also illustrates the surface length scales which are responsible for this signal, based on the same sensitivity calculation, but replacing LSTA with LSTA wavelet power. There is a consistent source of predictability from length scales ∼300 km throughout this period, whereas shorter length scales also contribute during the afternoon, when convective initiations peak. After sunset, the atmosphere gradually filters out smaller scale land information, consistent with an increasing role for horizontal advection in the nocturnal monsoon flow [49].

Figures 2(c)–(e) present the sensitivities for the Southern, Central and Northern Sahel by month. This shows that in the Southern Sahel, the sensitivity decreases as the season progresses, following a particularly strong signal in June. We ascribe this primarily to progressively smaller day-to-day variability in the surface energy balance, as quantified by the difference in LSTA between the 10th and 1st deciles ('dT' in the legend). Seasonally increasingly wetter soils and enhanced leaf area weaken the soil moisture control on ET, whilst the sensitivity of LST to ET is reduced with increasing vegetation cover. Both of these effects reduce our sensitivity metric as the season progresses. Consistent with figure 1(b), temporal variability in LSTA is higher in the Central and Northern Sahel, and this helps to explain the typically larger JJAS-mean sensitivities there compared to the Southern Sahel, particularly overnight. Note that during June, there is insufficient convection in the Northern Sahel to produce robust statistics.

We also assess the sensitivity of convection to sampling LSTA at locations up and downstream (to the east and west respectively) of the observed cores. Figure 2(f) shows that varying the sampling location of the LSTA by even 1° longitude (∼115 km) can substantially impact the sensitivity. During the early

Figure 2. Sensitivity (%) of cores to LSTA (K) based on data 2004–2015. (a) Frequency of cores observed within each LSTA decile at 1700 UTC. The distance along the red dashed line defines the sensitivity of cores to LSTA. Blue triangles denote observed soil moisture (m³ m⁻³) averaged over all days and locations in the control sample. (b) Sensitivity of cores to LSTA as a function of time since 1200 UTC (lower panel). Sensitivity of cores to LSTA variability at different length scales (km) and times of day (upper panel). Note that LSTA variability is normalised by its standard deviation for each length scale considered. Sensitivity of cores to LSTA by month for (c) 10–12.5° N, (d) 12.5–15° N, (e) 15–20° N. For each month, the difference in LSTA between the 10th and 1st deciles (dT; K) is given in the legend. (f) Sensitivity of cores to LSTA sampled at different longitudinal offsets. Apart from (c)–(e), the regressions are based on data from 10 to 20° N and months JJAS. Only sensitivities where the regression gradient is significantly positive ($P < 0.05$) are plotted in (b) and have squares in (c)–(f).

afternoon, when local initiation drives the increase in core frequency (figure 1(d)), the sensitivity is largest for the local LSTA. However, during the evening and overnight, when most convection is dominated by MCSs triggered to the east, we find that cores are favoured 100–200 km downstream of warmer surfaces. This result is entirely consistent with KT20,

where the passage of mature MCSs in late afternoon over drier soils favoured enhanced MCS rainfall in later hours, a signal still evident 600 km downstream. Importantly, the marked changes in sensitivity over sampling distances of around 100–200 km (figure 2(f)) implies that synoptic scale variability alone cannot explain our results.

4. Application of prototype tool for SWIFT Testbed

During the SWIFT Testbed, researchers and forecasters trialled new approaches in a quasi-operational forecasting environment. They sent bespoke nowcasting products to participating forecast users, who evaluated the products. To take advantage of this opportunity, we developed a simple prototype nowcasting tool. We translated each day's LSTA field into a 'Land Modification Factor' (LMF; %), defined as

$$\text{LMF} = \left(\text{LSTA} \times m_{i,j,k} + c_{i,j,k} - 10 \right) \times 10$$

where m and c are the gradient and intercept of the decile linear regression (figure 2) for time of day i, month j, and latitude band k. This factor expresses the climatological enhancement of core frequency for a given LSTA. For example, according to the linear regression in figure 2(a), an LSTA of $+5.9$ K (denoted by the upper red cross) has a core frequency of 14.1% per decile, giving an LMF of 41%. Every 15 min during the day, we produced LMF maps valid for each 3 h slot between 1200 and 0300 UTC the following day, using the latest LSTA. Informed by figure 2(f), the maps were computed with the decile regression for local LSTAs at 1200 and 1500 UTC forecast times, whilst for later times, we applied regressions using LSTAs 1° to the east. This simple approach implicitly distinguishes between times of day when storm initiation or propagation dominates. We also applied a linear weighting by latitude to smoothly adjust LMF values between the three Sahelian zones, and assumed an LMF of 0% (i.e. no effect) for cores south of 8.75° N.
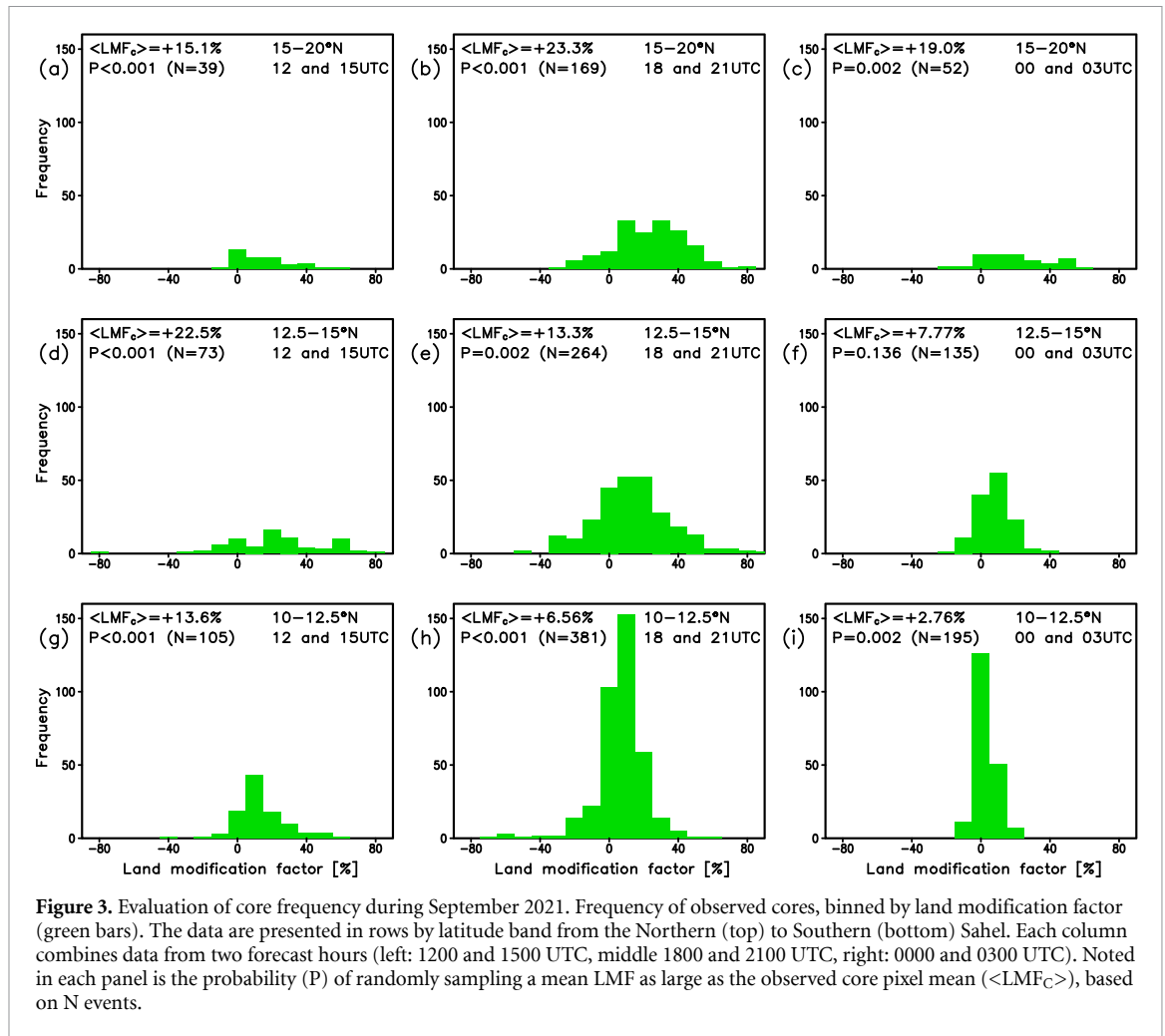
As a basic illustration of the skill of this method, figure 3 presents the frequency distribution of LMFs beneath each core observed during September 2021. Even from this relatively small sample size, and sampling data from outside the historical period, the distribution of cores is clearly skewed towards positive values of LMF. For each panel in figure 3, we compared the mean LMF to 10 000 samples of mean LMFs of the same size (N), drawn at random from the same latitude band and time of day, irrespective of core occurrence. In 11 of the 12 panels, the mean LMF was significantly larger (at the 1% level) than the domain as a whole. This indicates that our approach of using historical relationships to identify areas in NRT with higher likelihood of convection is robust.

By itself, the knowledge that convective cores are favoured over positive values of LMF is of limited help to a forecaster, because the majority of the region will not experience a core. The value of LMF maps for nowcasting emerges in combination with other data, notably NRT observations of convective activity and forecasts of the large-scale circulation. We next discuss how we used our LSTA-based approach to make manual nowcasts on a particular day. The cases are

illustrative of the coupled land-atmosphere processes that we observed throughout the Testbed and which, when aggregated together, produce the strong statistical signals evident in figures 2 and 3.

Figure 4 depicts conditions on 15 September 2021 when a major MCS affected the Western Sahel, whilst shorter-lived convective storms triggered along a line crossing Mali and Niger. According to IMERG, 12 h rainfall to midnight exceeded 100 mm in parts of Mali, Mauretania and Senegal, with a maximum of 220 mm around 14° W, 15° N (figure 4(a)). The MCS responsible for these totals initiated at 'A' in Western Mali around midday, as a 'parent' MCS decayed to the south at 'Z'. During the day, two convergence lines (indicated by narrow discontinuous bands of initially shallow cloud) ran north-eastwards away from the initiation zone (figure 4(b)), arcing back via 'E' and 'F' as far as south-eastern Niger ('G'), some 2500 km away. Similar convergence lines, often linked to the ITD, were frequently observed by a research radar based in Niamey during the AMMA field campaign [50].
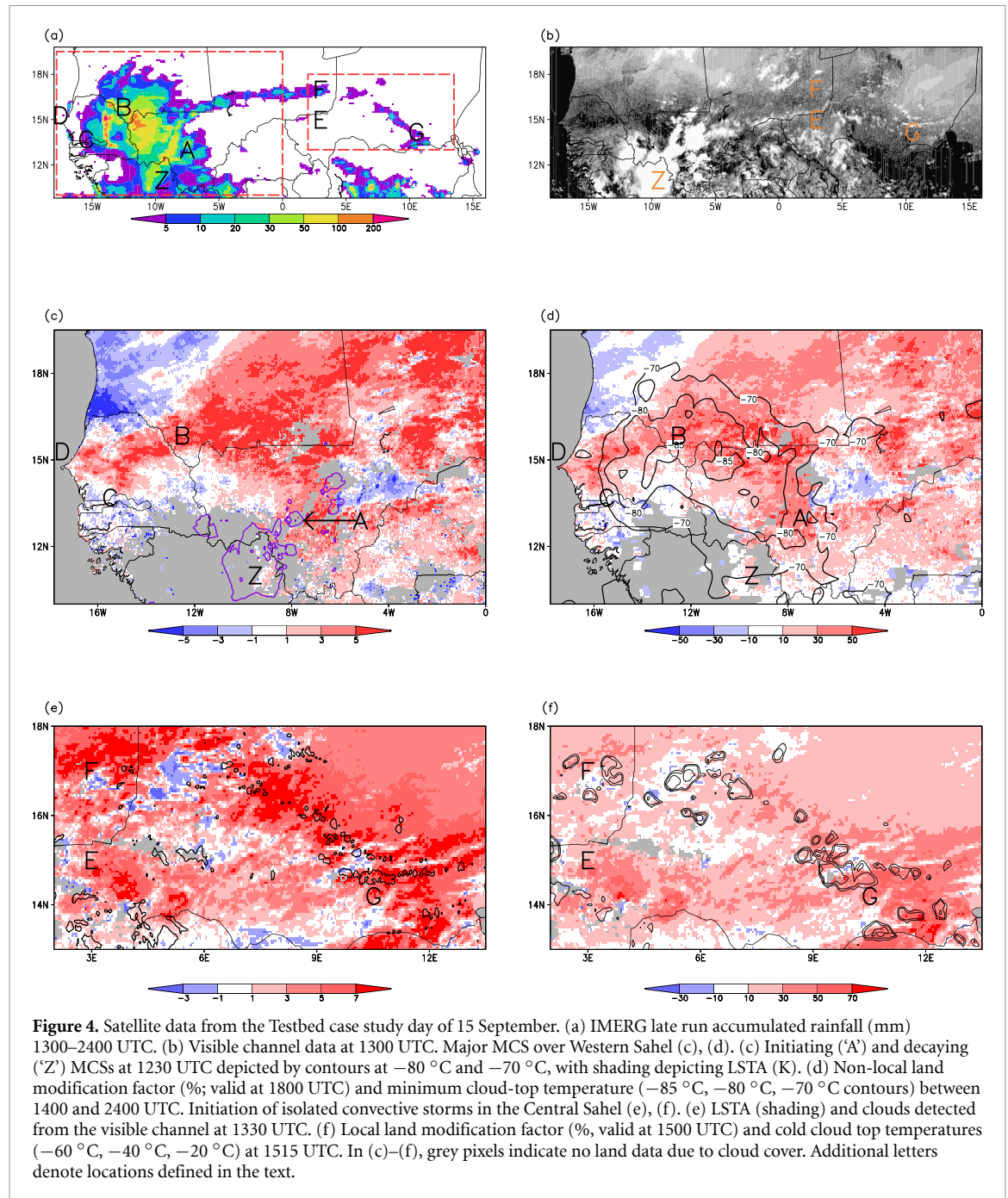
The first deep convection in what became the major MCS appeared at 1130 UTC, yet by 1230 UTC (figure 4(c)), the cloud area colder than -70 C already exceeded 4000 km^2, with a minimum pixel temperature of -90.5 C. That indicated a particularly vigorous system given the time of day [11], and therefore the MCS seemed likely to propagate well into the evening. Convection initiated within a slot of warm LSTAs which stretched north into Mauritania (approximately 10° W–6° W; figure 4(c)). According to IMERG, this slot had received no rain in the previous five days, in contrast to rainier conditions to the west and east. As demonstrated by KT20, on scales of several hundred kilometres, anomalously dry surfaces provide ideal conditions for MCS intensification, through enhanced convergence and wind shear. Translating the LSTA data into a map of LMF (valid for 1800 UTC), the region to the north-west of the initiation had an enhancement factor of around $+40$% as compared to -10% LMF for the region to the west (figure 4(d)). Further west still, a wet surface in SW Mauritania and the far north of Senegal contrasted with warmer, drier conditions in Central Senegal, with typical LMFs of -20 to $+30$% respectively. Based on the vigour of the new system and the LSTA maps, in the early afternoon we predicted that the MCS would favour a north-westward path over the drier surface, and if it were still active by the time it reached Senegal, it could change to a more south-westward direction towards the Dakar Peninsula ('D'). Note that whilst the Global Forecast System (GFS) forecast from 0600 UTC that day indicated moderately high shear over Western Mali and Senegal, the predicted direction of the AEJ was towards the WSW direction, and so unlikely to favour propagation towards the north-west. In reality, the MCS did follow the somewhat unusual trajectory that

Figure 3. Evaluation of core frequency during September 2021. Frequency of observed cores, binned by land modification factor (green bars). The data are presented in rows by latitude band from the Northern (top) to Southern (bottom) Sahel. Each column combines data from two forecast hours (left: 1200 and 1500 UTC, middle 1800 and 2100 UTC, right: 0000 and 0300 UTC). Noted in each panel is the probability (P) of randomly sampling a mean LMF as large as the observed core pixel mean (<LMF$_C$>), based on N events.

we had predicted, changing direction from north-westerly to south-westerly as it approached the Senegalese border (point 'B') around 1800 UTC. By that time, based on favourable LMF patterns, we predicted that the system could reach the heavily populated coast (including Dakar) overnight. At 2330 UTC, the Senegalese forecast centre ANACIM issued an SMS warning to around 40 000 people of thunderstorms and strong winds. In reality, the system split into two around 0100 UTC, with the southern MCS bringing heavy rain across Central and South-Western Senegal (centred around 'C'), and the northern storm weakening as it approached the coastline around the Senegal-Mauretania border. By this time of night, differences in LMF across Senegal were relatively weak ($\pm 20\%$, not shown) and the effects of the nearby ocean may also have played a role in degrading land-based skill. However, even at 0300 UTC, the cloud area at a threshold of $-75\,^\circ$C exceeded 50 000 km^2, indicating a particularly intense MCS according to the climatology of [18].

Whilst the above nowcast was made once the MCS was initiated, on the same day we also made predictions for locations in Niger where new MCSs could be triggered. These were based on the presence of the extended convergence lines noted above, in combination with a heterogeneous soil moisture pattern. By 1330 UTC, shallow clouds with temperatures of $+10\,^\circ$C–$0\,^\circ$C were starting to emerge, organised by the two convergence lines running via F and E across the region to point G (figure 4(e)). At finer scales within the bands, the developing convection tended to appear above warmer (drier) surfaces (e.g. at 9° E, 16° N), often near boundaries with cooler (wetter) soil (e.g. around 10° E, 15° N). From numerical model simulations, we know that such structures are typical for the development of convection embedded within soil moisture-forced boundary layer circulations [51]. By 1515 UTC (figure 4(f)), deep convection had triggered in a number of these locations within the northern line. These storms were relatively short-lived but were responsible for the linear rainfall structure linking 'Z' to 'G' via 'F' (figure 4(a)). Throughout the Testbed, we found that the combination of convergence lines and surface patchiness frequently triggered deep convection in the Niger/Mali region. By combining land and cloud observations, such favoured locations could be identified up to 2 h ahead of triggering, giving forecasters a head-start in providing local-scale nowcasts.

Figure 4. Satellite data from the Testbed case study day of 15 September. (a) IMERG late run accumulated rainfall (mm) 1300–2400 UTC. (b) Visible channel data at 1300 UTC. Major MCS over Western Sahel (c), (d). (c) Initiating ('A') and decaying ('Z') MCSs at 1230 UTC depicted by contours at −80 °C and −70 °C, with shading depicting LSTA (K). (d) Non-local land modification factor (%; valid at 1800 UTC) and minimum cloud-top temperature (−85 °C, −80 °C, −70 °C contours) between 1400 and 2400 UTC. Initiation of isolated convective storms in the Central Sahel (e), (f). (e) LSTA (shading) and clouds detected from the visible channel at 1330 UTC. (f) Local land modification factor (%, valid at 1500 UTC) and cold cloud top temperatures (−60 °C, −40 °C, −20 °C) at 1515 UTC. In (c)–(f), grey pixels indicate no land data due to cloud cover. Additional letters denote locations defined in the text.

5. Discussion and summary

In this study, we have quantified a strong signal linking positive LSTAs with subsequent intense convection within MCSs in the Sahel. This sensitivity extends well beyond the afternoon period when land-atmosphere feedbacks are expected to be maximised. Warmer surface features on length scales of several hundred kilometres contribute to the maintenance of predictive skill overnight, whilst the impacts of smaller scale land variability gradually weaken during the evening. Physically, enhanced LSTAs indicate areas where ET is more moisture-stressed than usual, with much of the excess surface energy warming the boundary layer. The importance of LSTA

variability on scales of several hundred kilometres is consistent with KT20; propagating MCSs tend to weaken over wetter surfaces and intensify over drier soils. Favourable (dry) upstream soil conditions increase the likelihood of an MCS propagating further overnight. The combination of storms which are both long-lived and sensitive to slowly varying land state opens up the possibility for skilful nowcasting of MCSs tracks out to many hours, substantially longer than conventionally attempted [32, 39].

We have documented how we used land surface information to make subjective forecasts on one day. Supplementary figure 1 (available online at stacks.iop.org/ERL/17/034016/mmedia) provides

a summary map of cores and LMFs and a simple statistical evaluation for each day of the Testbed. With a rather limited sample of cores, one would not expect a robust statistical signal every day. Somewhat surprisingly however, the signal was evident at the 99% level on five of the twelve Testbed days. Statistical significance tended to be weaker on days where convection was predominantly in the Southern Sahel, which is to be expected given the relatively weak sensitivity in that region (figure 2(c)). Indeed comparison of the sensitivity with other months (figure 2) suggests that LSTA-based forecast skill across the Sahel, however quantified, would be stronger earlier in the wet season. On the other hand, our reliance on the availability of cloud-free LST data will limit the utility of this approach at the height of the wet season, particularly in the Southern Sahel.

We have illustrated how land surface information can improve manual nowcasts of severe weather, particularly on scales of tens of kilometres. Reliable prediction at such scales is well beyond the capabilities of current NWP systems in the Sahel, at least in areas lacking strong orographic or coastal forcing. A recent West African study [27] also showed how forecasting based solely on antecedent rainfall outperforms predictions from a state-of-the-art ensemble forecasting system. Information on antecedent rain (via its impact on the surface energy balance) is implicit in our approach, as is the effect of synoptic rainfall organisation highlighted in their analysis. We find skill from land features on scales of 10 s km during the afternoon, and 100–200 km overnight, which cannot be explained by synoptic processes. Taken together, these two studies suggest there is substantial scope for improving early warning of hydro-meteorological hazards in the region. Our proof-of-concept study provides encouragement for the development of more automated tools, for example the incorporation of land information into forward propagation methods, and machine-learning approaches. There are several aspects where the nature of that land information could be optimised, for example by tuning the location of the upstream LSTA target and filtering out fine scale land features within overnight nowcasts, by re-introducing elements of the climatological LST field associated with significant mesoscale landscape features such as wetlands and urban areas, and by bringing in microwave soil moisture retrievals to overcome cloud cover issues. Such advances could be extremely valuable for West African decision-makers in sectors including civil defence, agriculture, travel, and aviation. Beyond West Africa, and depending on the strength of soil moisture-MCS coupling, there is also potential for applying these techniques in other semi-arid regions where existing forecasts are poor.

ORCID iDs

Christopher M Taylor ⦿ https://orcid.org/0000-0002-0120-3198
Cornelia Klein ⦿ https://orcid.org/0000-0001-6686-0458
Cheikh Dione ⦿ https://orcid.org/0000-0002-8457-6175
Douglas J Parker ⦿ https://orcid.org/0000-0003-2335-8198
John Marsham ⦿ https://orcid.org/0000-0003-3219-8472
Cheikh Abdoulahat Diop ⦿ https://orcid.org/0000-0001-9309-885X
Jennifer Fletcher ⦿ https://orcid.org/0000-0002-4892-3344
Abdoul Aziz Saidou Chaibou ⦿
https://orcid.org/0000-0002-0560-7050
Valiyaveetil Shamsudheen Semeena ⦿
https://orcid.org/0000-0002-1895-449X
Steven J Cole ⦿ https://orcid.org/0000-0003-4294-8687
Seonaid R Anderson ⦿ https://orcid.org/0000-0001-8556-577X

References

[1] Dirmeyer P A, Halder S and Bombardi R 2018 On the harvest of predictability from land states in a global forecast model *J. Geophys. Res.: Atmos.* **123** 13–111
[2] Koster R *et al* 2011 The second phase of the global land–atmosphere coupling experiment: soil moisture contributions to subseasonal forecast skill *J. Hydrometeorol.* **12** 805–22
[3] Koster R D *et al* 2004 Regions of strong coupling between soil moisture and precipitation *Science* **305** 1138–40
[4] Taylor C M, de Jeu R A M, Guichard F, Harris P P and Dorigo W A 2012 Afternoon rain more likely over drier soils *Nature* **489** 423–6
[5] Dirmeyer P A 2011 The terrestrial segment of soil moisture-climate coupling *Geophys. Res. Lett.* **38** L16702
[6] Seneviratne S I *et al* 2010 Investigating soil moisture-climate interactions in a changing climate: a review *Earth-Sci. Rev.* **99** 125–61
[7] Findell K L and Eltahir E A B 2003 Atmospheric controls on soil moisture-boundary layer interactions. Part I: framework development *J. Hydrometeorol.* **4** 552–69

[8] Guillod B P, Orlowsky B, Miralles D G, Teuling A J and Seneviratne S I 2015 Reconciling spatial and temporal soil moisture effects on afternoon rainfall *Nat. Commun.* **6** 6443

[9] Lohou F *et al* 2014 Surface response to rain events throughout the West African monsoon *Atmos. Chem. Phys.* **14** 3883–98

[10] Mathon V, Laurent H and Lebel T 2002 Mesoscale convective system rainfall in the Sahel *J. Appl. Meteorol.* **41** 1081–92

[11] Futyan J M and Genio A D D 2007 Deep convective system evolution over Africa and the tropical Atlantic *J. Clim.* **20** 5041–60

[12] Taylor C M, Parker D J and Harris P P 2007 An observational case study of mesoscale atmospheric circulations induced by soil moisture *Geophys. Res. Lett.* **34** L15801

[13] Taylor C M *et al* 2011 Frequency of Sahelian storm initiation enhanced over mesoscale soil-moisture patterns *Nat. Geosci.* **4** 430–3

[14] Gantner L and Kalthoff N 2010 Sensitivity of a modelled life cycle of a mesoscale convective system to soil conditions over West Africa *Q. J. R. Meteorol. Soc.* **136** 471–82

[15] Klein C and Taylor C M 2020 Dry soils can intensify mesoscale convective systems *Proc. Natl Acad. Sci.* **117** 21132–7

[16] Cook K H 1999 Generation of the African easterly jet and its role in determining West African precipitation *J. Clim.* **12** 1165–84

[17] Vizy E K and Cook K H 2018 Mesoscale convective systems and nocturnal rainfall over the West African Sahel: role of the inter-tropical front *Clim. Dyn.* **50** 587–614

[18] Taylor C M *et al* 2017 Frequency of extreme Sahelian storms tripled since 1982 in satellite observations *Nature* **544** 475–8

[19] Taylor C M, Parker D J, Lloyd C R and Thorncroft C D 2005 Observations of synoptic scale land surface variability and its coupling with the atmosphere *Q. J. R. Meteorol. Soc.* **131** 913–38

[20] Parker D J 2008 A simple model of coupled synoptic waves in the land surface and atmosphere of the northern Sahel *Q. J. R. Meteorol. Soc.* **134** 2173–84

[21] di Baldassarre G, Montanari A, Lins H, Koutsoyiannis D, Brandimarte L and Blöschl G 2010 Flood fatalities in Africa: from diagnosis to mitigation *Geophys. Res. Lett.* **37** L22402

[22] Panthou G *et al* 2018 Rainfall intensification in tropical semi-arid regions: the Sahelian case *Environ. Res. Lett.* **13** 064013

[23] Klein C *et al* 2021 Combining CMIP data with a regional convection-permitting model and observations to project extreme rainfall under climate change *Environ. Res. Lett.* **16** 104023

[24] Berthou S, Kendon E J, Rowell D P, Roberts M J, Tucker S and Stratton R A 2019 Larger future intensification of rainfall in the West African Sahel in a convection-permitting model *Geophys. Res. Lett.* **46** 13299–307

[25] Vogel P, Knippertz P, Fink A H, Schlueter A and Gneiting T 2018 Skill of global raw and postprocessed ensemble predictions of rainfall over northern tropical Africa *Weather Forecast.* **33** 369–88

[26] Baumgart M, Ghinassi P, Wirth V, Selz T, Craig G C and Riemer M 2019 Quantitative view on the processes governing the upscale error growth up to the planetary scale using a stochastic convection scheme *Mon. Weather Rev.* **147** 1713–31

[27] Vogel P, Knippertz P, Gneiting T, Fink A H, Klar M and Schlueter A 2021 Statistical forecasts for the occurrence of precipitation outperform global models over northern tropical Africa *Geophys. Res. Lett.* **48** e2020GL091022

[28] Yano J-I *et al* 2018 Scientific challenges of convective-scale numerical weather prediction *Bull. Am. Meteorol. Soc.* **99** 699–710

[29] Wilson J, Megenhardt D and Pinto J 2020 NWP and radar extrapolation: comparisons and explanation of errors *Mon. Weather Rev.* **148** 4783–98

[30] Jones T A, Knopfmeier K, Wheatley D, Creager G, Minnis P and Palikonda R 2016 Storm-scale data assimilation and ensemble forecasting with the NSSL experimental warn-on-forecast system. Part II: combined radar and satellite data experiments *Weather Forecast.* **31** 297–327

[31] Fabry F and Meunier V 2020 Why are radar data so difficult to assimilate skillfully? *Mon. Weather Rev.* **148** 2819–36

[32] Roberts A J *et al* 2021 Nowcasting for Africa: advances, potential and value *Weather* (https://doi.org/10.1002/wea.3936)

[33] Kolios S and Feidas H 2013 An automated nowcasting system of mesoscale convective systems for the Mediterranean basin using Meteosat imagery. Part I: system description *Meteorol. Appl.* **20** 287–95

[34] Pulkkinen S *et al* 2019 Pysteps: an open-source Python library for probabilistic precipitation nowcasting (v1.0) *Geosci. Model Dev.* **12** 4185–219

[35] Ravuri S *et al* 2021 Skilful precipitation nowcasting using deep generative models of radar *Nature* **597** 672–7

[36] Chen L, Cao Y, Ma L and Zhang J 2020 A deep learning-based methodology for precipitation nowcasting with radar *Earth Space Sci.* **7** e2019EA000812

[37] James P M, Reichert B K and Heizenreder D 2018 NowCastMIX: automatic integrated warnings for severe convection on nowcasting time scales at the German Weather Service *Weather Forecast.* **33** 1413–33

[38] Parker D J *et al* 2021 The African SWIFT project: growing science capability to bring about a revolution in weather prediction *Bull. Am. Meteorol. Soc.* 1–53

[39] Hill P G, Stein T H M, Roberts A J, Fletcher J K, Marsham J H and Groves J 2020 How skilful are nowcasting satellite applications facility products for tropical Africa? *Meteorol. Appl.* **27** e1966

[40] Burton R R *et al* 2022 Satellite-based nowcasting of West African mesoscale storms has skill at up to four hours lead time *Weather Forecast.* (https://doi.org/10.1175/WAF-D-21-0051.1)

[41] WMO 2017 *Guidelines for Nowcasting Techniques* (Geneva: World Meteorological Organisation)

[42] Klein C, Belušić D and Taylor C M 2018 Wavelet scale analysis of mesoscale convective systems for detecting deep convection from infrared imagery *J. Geophys. Res.: Atmos.* **123** 3035–50

[43] Sobrino J A and Romaguera M 2004 Land surface temperature retrieval from MSG1-SEVIRI data *Remote Sens. Environ.* **92** 247–54

[44] Anderson M and Kustas W 2008 Thermal remote sensing of drought and evapotranspiration *Eos Trans. Am. Geophys. Union* **89** 233

[45] Fisher J B *et al* 2020 ECOSTRESS: NASA's next generation mission to measure evapotranspiration from the international space station *Water Resour. Res.* **56** e2019WR026058

[46] Carlson T 2007 An overview of the 'triangle method' for estimating surface evapotranspiration and soil moisture from satellite imagery *Sensors* **7** 1612–29

[47] Gallego-Elvira B, Taylor C M, Harris P P, Ghent D, Veal K L and Folwell S S 2016 Global observational diagnosis of soil moisture control on the land surface energy balance *Geophys. Res. Lett.* **43** 2623–31

[48] Owe M, de Jeu R and Holmes T 2008 Multisensor historical climatology of satellite-derived global land surface moisture *J. Geophys. Res.-Earth Surf.* **113**

[49] Parker D J *et al* 2005 The diurnal cycle of the West African monsoon circulation *Q. J. R. Meteorol. Soc.* **131** 2839–60

[50] Dione C *et al* 2013 Phenomenology of Sahelian convection observed in Niamey during the early monsoon *Q. J. R. Meteorol. Soc.* 500–16

[51] Rieck M, Hohenegger C and van Heerwaarden C C 2014 The influence of land surface heterogeneities on cloud size development *Mon. Weather Rev.* **142** 3830–46